NASA/TM–2010-216859

Evaluation of Acoustic Emission NDE of Composite Crew Module Service Module / Alternate Launch Abort System (CCM SM/ALAS) Test Article Failure Tests

Michael R. Horne
National Institute of Aerospace, Hampton, Virginia

Eric I. Madaras
Langley Research Center, Hampton, Virginia

October 2010

NASA STI Program . . . in Profile

Since its founding, NASA has been dedicated to the advancement of aeronautics and space science. The NASA scientific and technical information (STI) program plays a key part in helping NASA maintain this important role.

The NASA STI program operates under the auspices of the Agency Chief Information Officer. It collects, organizes, provides for archiving, and disseminates NASA's STI. The NASA STI program provides access to the NASA Aeronautics and Space Database and its public interface, the NASA Technical Report Server, thus providing one of the largest collections of aeronautical and space science STI in the world. Results are published in both non-NASA channels and by NASA in the NASA STI Report Series, which includes the following report types:

- TECHNICAL PUBLICATION. Reports of completed research or a major significant phase of research that present the results of NASA programs and include extensive data or theoretical analysis. Includes compilations of significant scientific and technical data and information deemed to be of continuing reference value. NASA counterpart of peer-reviewed formal professional papers, but having less stringent limitations on manuscript length and extent of graphic presentations.

- TECHNICAL MEMORANDUM. Scientific and technical findings that are preliminary or of specialized interest, e.g., quick release reports, working papers, and bibliographies that contain minimal annotation. Does not contain extensive analysis.

- CONTRACTOR REPORT. Scientific and technical findings by NASA-sponsored contractors and grantees.

- CONFERENCE PUBLICATION. Collected papers from scientific and technical conferences, symposia, seminars, or other meetings sponsored or co-sponsored by NASA.

- SPECIAL PUBLICATION. Scientific, technical, or historical information from NASA programs, projects, and missions, often concerned with subjects having substantial public interest.

- TECHNICAL TRANSLATION. English-language translations of foreign scientific and technical material pertinent to NASA's mission.

Specialized services also include creating custom thesauri, building customized databases, and organizing and publishing research results.

For more information about the NASA STI program, see the following:

- Access the NASA STI program home page at *http://www.sti.nasa.gov*

- E-mail your question via the Internet to help@sti.nasa.gov

- Fax your question to the NASA STI Help Desk at 443-757-5803

- Phone the NASA STI Help Desk at 443-757-5802

- Write to:
  NASA STI Help Desk
  NASA Center for AeroSpace Information
  7115 Standard Drive
  Hanover, MD 21076-1320

NASA/TM–2010-216859

Evaluation of Acoustic Emission NDE of Composite Crew Module Service Module / Alternate Launch Abort System (CCM SM/ALAS) Test Article Failure Tests

Michael R. Horne
National Institute of Aerospace, Hampton, Virginia

Eric I. Madaras
Langley Research Center, Hampton, Virginia

National Aeronautics and
Space Administration

Langley Research Center
Hampton, Virginia 23681-2199

October 2010

Available from:

NASA Center for AeroSpace Information
7115 Standard Drive
Hanover, MD 21076-1320
443-757-5802

Table of Contents

Table of Figures

Symbols and Abbreviations

CCM	Composite Crew Module
SM	Service Module
ALAS	Alternate Launch Abort System
NDE	Nondestructive Evaluation
AE	Acoustic emission

Abstract

Failure tests of CCM SM/ALAS (Composite Crew Module Service Module / Alternate Launch Abort System) composite panels were conducted during 7/10/2008 and 7/24/2008 at LaRC. This is a report of the analysis of the Acoustic Emission (AE) data collected during those tests.

1.0 Introduction

This is a report of the investigation of the Acoustic Emission (AE) data collected during the failure tests of CCM SM/ALAS composite panels. As stated in the test plan, "The Composite Crew Module (CCM) SM/ALAS fittings provide a common interface for reacting loads from two major load cases; connecting to the Service Module (SM) during launch and the Alternate Launch Abort System (ALAS) during abort. The large loads reacted through these fittings makes the SM/ALAS region a critical area in the CCM design and therefore a component test will be performed. [1]" This test component is a simplified version of a portion of the CCM shell, backbone fittings and the SM/ALAS fittings. The fittings are metallic and the shell portion is a complex sandwich panel of composite laminate face sheets and honeycomb metallic core tapering into a solid laminate-only region where the metallic fittings are bolted. This report discusses two panels that were tested. The test plan states that, "load shall be applied in increments to hold points at 3, 8, 33, 66, and 100 kips holding for one minute and returning to zero after each hold to check for hysteresis." Any deviations from that procedure that was relevant to AE generation will be noted.

2.0 AE Test Configuration

Figures 1, 2, and 3 are schematics from the test plan [1]. They show the general dimensions of the panels and configuration of the load test. See the test plan for further details of the test.

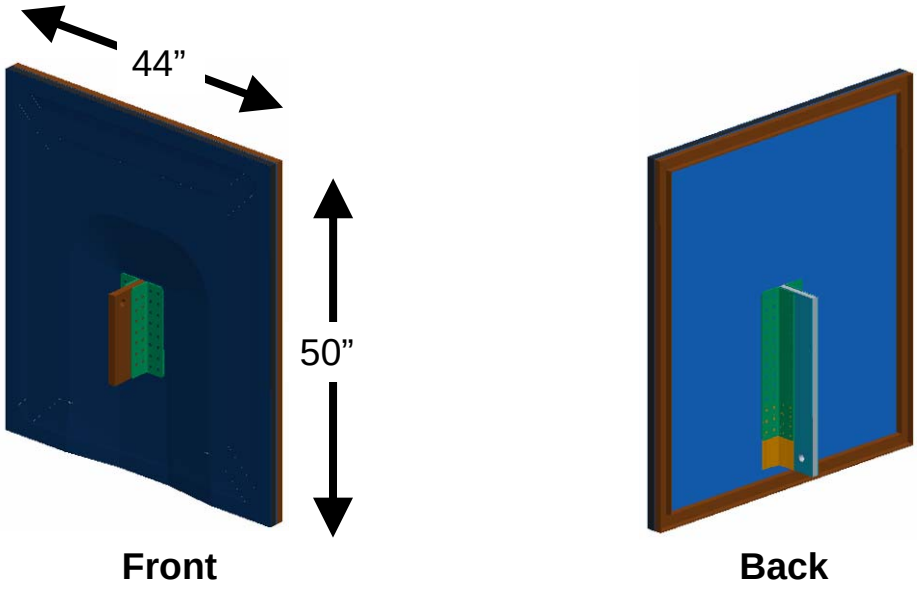

Figure 1 – Simplified SM/ALAS Test Article Geometry

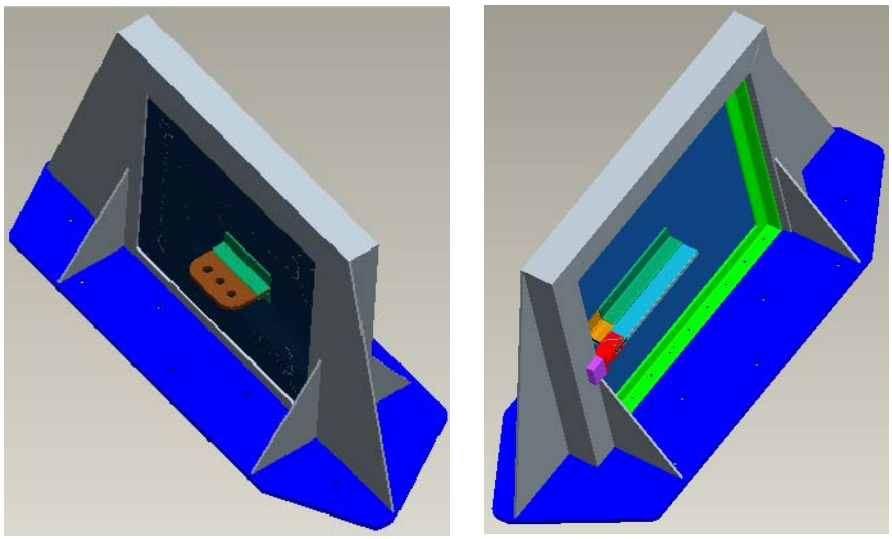

Figure 2 – Loading and Support Structure for Simplified SM/ALAS Test Article

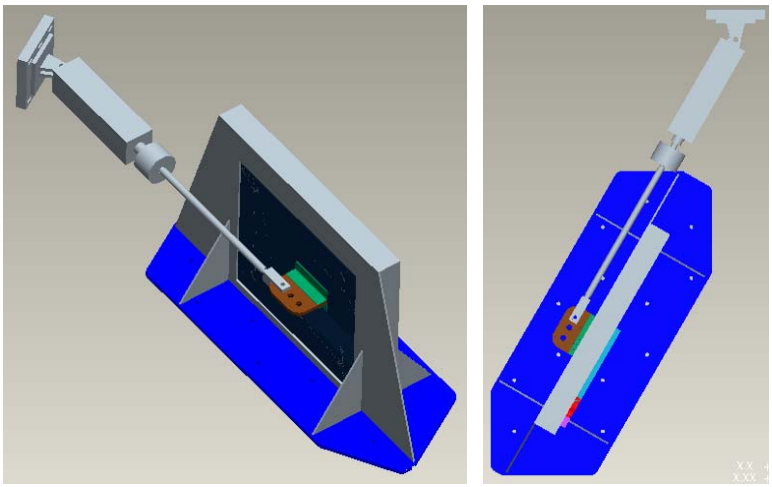

Figure 3 – Loading Configuration for SM/ALAS Test Article

AE Instrumentation on test article:

Several acoustic emission sensors (Digital Wave B1025) were mounted on the back, front, and to the stiffeners of the Composite Crew Module SM-ALAS test article approximately as shown in Figure 4. Additional sensors, changes, and exact locations will be noted in later sections for each panel test. All sensors were bonded with Lord 202 acrylic adhesive onto metal tape that was attached to the test article for easy removal.

All transducers were connected to thin BNC sensor cables, which in turn were connected to Digital Wave PA0 preamp/line drivers. The preamps were connected via long BNC cables to a remotely located Digital Wave FM1 signal conditioning 16-channel amplifier. The data was recorded for subsequent processing on a computer using Digital Wave data acquisition software. The processing was done with the same software.

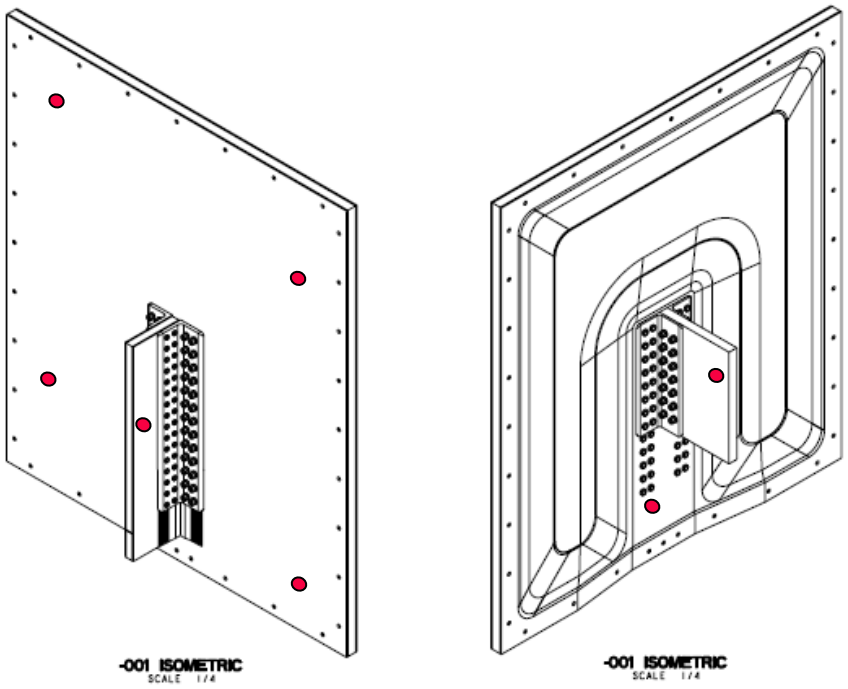

Figure 4 – Approximate locations of AE sensors (red dots) to be mounted on the CCM SM-ALAS

3.0 Analysis and results

AE systems collect structure-borne sound generated by dynamic processes occurring in or impinging on the structure. Data from a network of sensors can be used to locate the epicenter of the process by triangulation using time-of-flight of the sound from the source to the sensors. Also recorded is the time each event occurs, so one can plot the event rate (event per unit time).

Energy calculations can be applied to each waveform collected by each sensor. The result is a function of the energy of the signal collected at each sensor and is therefore related to the energy release of each event, but also includes the transfer function of the material (attenuation, filtering, reflection, etc.) during propagation from source to sensor and the transfer function of the sensor. The event energy calculations can be plotted by channel (sensor) in energy vs. time plots. With further filtering and manipulation the signal energy can also be indicated on the event rate plots for each event.

Methods for testing and field calibrating AE sensor installations require the use of an artificial AE source. For most situations it has been found that by pressing a mechanical pencil lead on the surface of a specimen, at an angle to the surface, until the pencil lead breaks, can create a set of transient waves traveling along the surface and into the bulk that mimic an AE event. If the lead is of a particular hardness and diameter with a specific length that is unsupported (length sticking out from metal sheath of mechanical pencil) and held at a particular angle, the break is a very repeatable transient forcing function on the surface of the specimen. Even if the effort to get repeatability is not followed, pencil lead breaking can be a very effective method for testing whether sensors, cabling, or electronics are working or estimate how well bonded the sensor is to the specimen. If the lead breaks are performed at known locations, typically beside each sensor in the network, one can estimate wave speeds in the test specimen from the data, for use in event location calculations.

The accuracy of event location calculations will depend on knowing the velocity of the AE wave propagation accurately. The simplest unbounded materials are homogeneous and isotropic and have three modes of wave travel. Boundaries support many other modes (plate, surface, etc.). Wave propagation can also be dispersive: velocity is a function of frequency. Hence, wave velocity can be a function of where the wave is traveling in a material, what direction it is traveling, and its mode of travel (characteristic pattern of particle displacements as wave propagates). These test panels are complex, bounded, inhomogeneous, and anisotropic structures made from various materials that potentially can create and sustain many different modes, frequencies and, hence, velocities of propagation. Damage introduces changes in material and mechanical properties of the panel that can further affect propagation velocity. Also, there are the data analyses issues of trying to algorithmically decide what the arrival time of an event signal is, which can be difficult for dispersive waves. **So, individual event location for a complex structure such as these panels is, at best, an estimate.** One needs to look at the clustering and patterning of significant quantities of events, instead of individual ones.

The two panels tested were not constructed exactly the same [3]. The core in the tapered region of panel 2 was potted. In addition, panel 2 had some manufacturing flaws (weak skin/core interface) which were unknown at the time of testing. Existence of these flaws is supported by the analysis of the AE results discussed in section 3.2. Panel 2 also had fiber optic sensors mounted to it, but they should not have contributed to the difference in response of the panels to

load.

3.1 Panel 1 Analysis

The following figures 5 and 6 of test panel 1 mounted in the load frame are annotated with the locations of the AE sensors. Note that sensors 5, 6, and 7 are located nearest to the bolts and brackets.

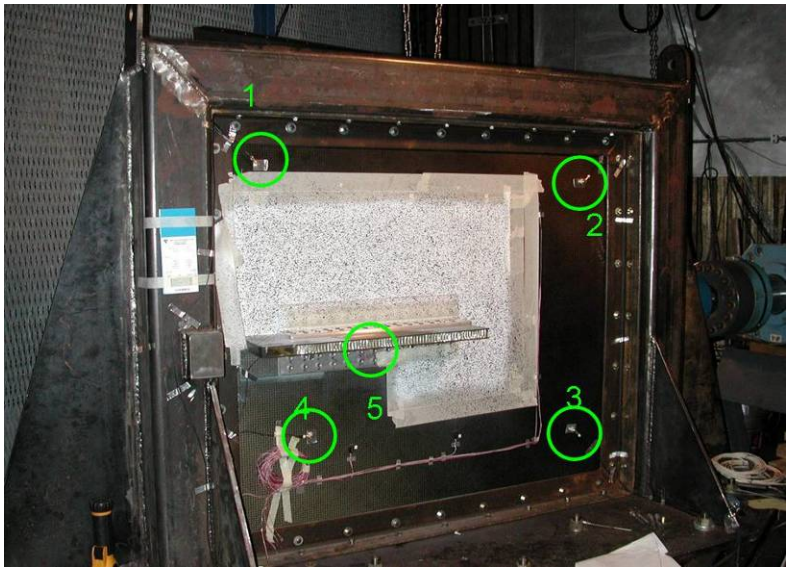

Figure 5 – AE Sensor locations on the back side of panel 1 in test frame

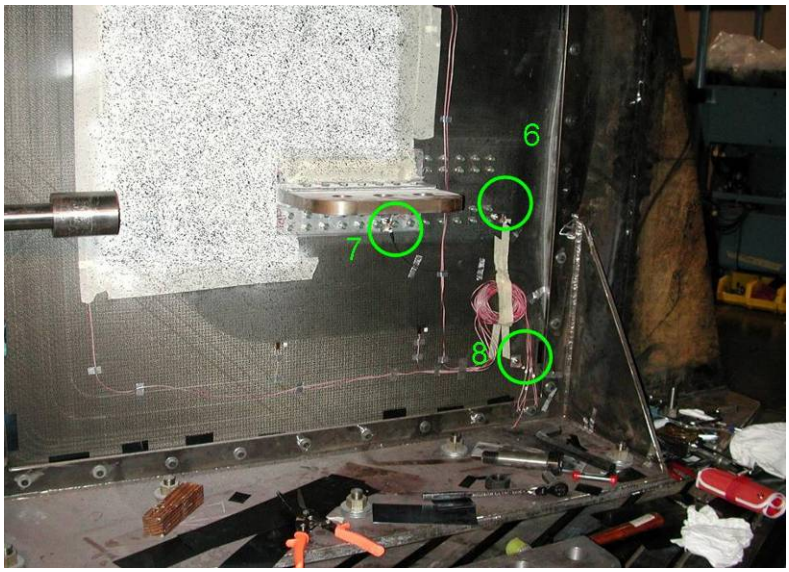

Figure 6 – AE Sensor locations on the front side of panel 1 in test frame.

The plot in figure 7 of AE events, plotted against the load profiles that panel 1 was subjected to, shows how the Kaiser effect applies to this test. The Kaiser effect is related to "conditioning" of

a material during loading. [2] It states that if no damage has occurred since a previous load cycle, then acoustic emission should not occur during a subsequent load cycle until the peak load of the previous cycle has been reached. It is primarily valid for metallic materials in which dislocation acceleration and inclusion fractures are the primary AE sources. It is only approximate for composite materials due to their more complex internal structure, which leads to more internal friction and other interferences that can occur during post-damage loading and unloading and is known as the Felicity Effect. [2] Hence, some AE may occur upon reloading at loads lower than previous peak. For this test it does indeed look like the Kaiser effect is valid for the first three load cycles. However what we see in run 4 is that the AE rate increases when the load reaches the previous peak, even though some AE was occurring prior to that.

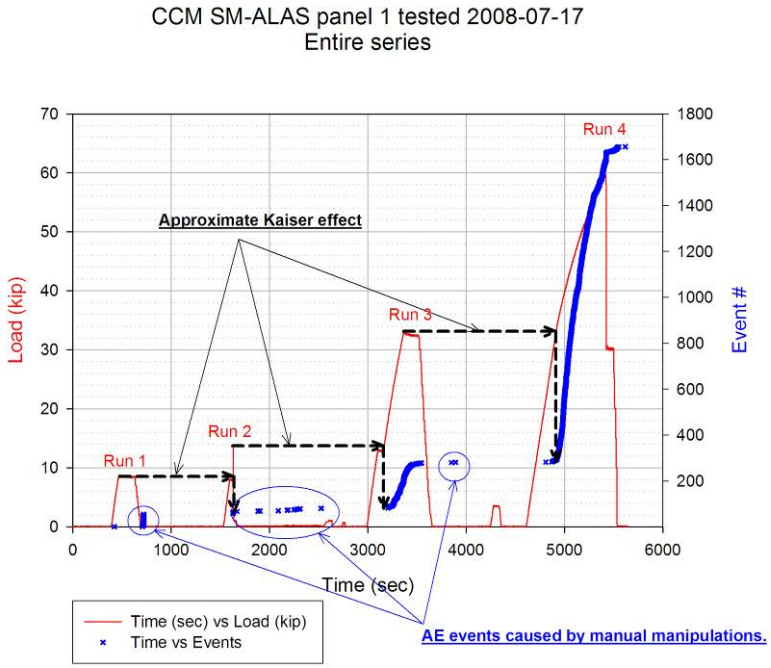

Figure 7 – Acoustic emission rate vs. load profile and Kaiser effect

Because panel 1 failed in the metallic fittings it was conjectured that most of the AE was due to bracket and bolt noise, while a relatively small amount of damage occurred in the composite. It should be noted that sensor 7 was the only sensor located on the metal brackets as seen in figure 8. Sensor 5 was mounted on the composite stiffener opposite the clevis bracket and sensor 6 was mounted near the bolts, but on the composite skin as seen in figures 9 and 10, respectively. Sensors 5 and 6 would be less sensitive to bolt and bracket noise than sensor 7, but presumably more sensitive than other sensors further away. The metallic bracket failure conjecture is supported by figures 11 and 12, which show the event time of the first sensor arrival and the histogram of the first arrival event count, both plotted per channel (sensor). It is shown that the majority of the events occur near the bracket mounted sensor 7, suggesting that the bracket was failing. Also, a significant burst of that AE occurred in Run 3 at loads between 15 and 30 kips. The percentage of first arrival hits at sensor 8 comes in second after sensor 7 for both runs. Since

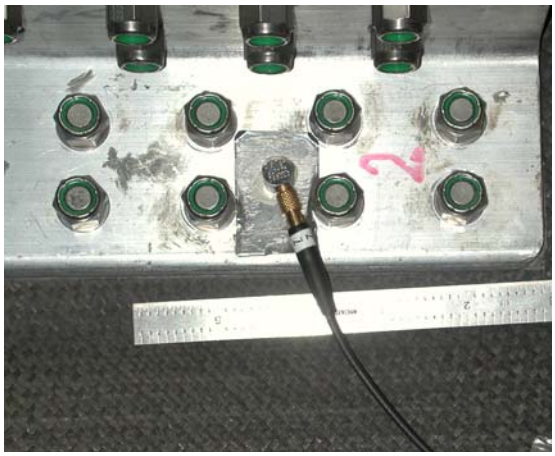

Figure 8 Close-up of sensor 7 location.

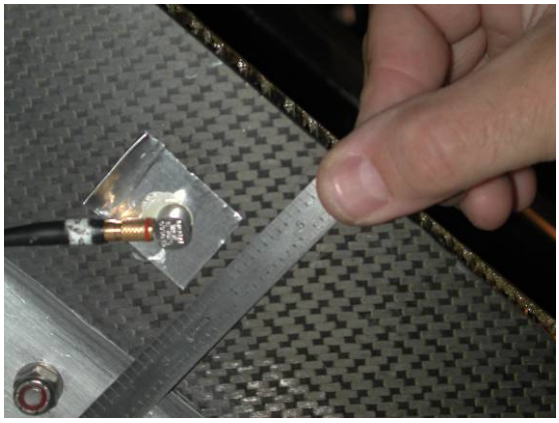

Figure 9 Close-up of sensor 5 looking up at bottom surface of stiffener

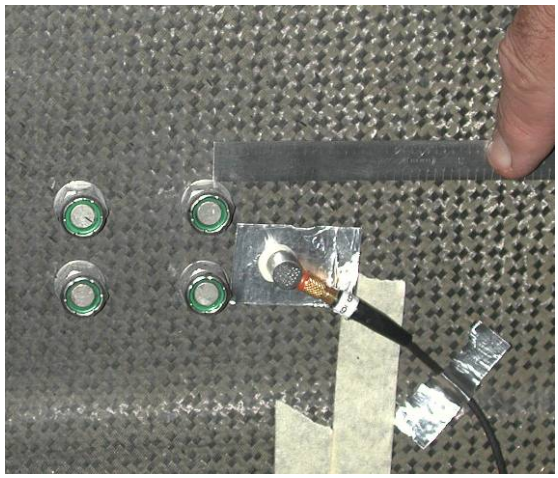

Figure 10 Close-up of sensor 6 location.

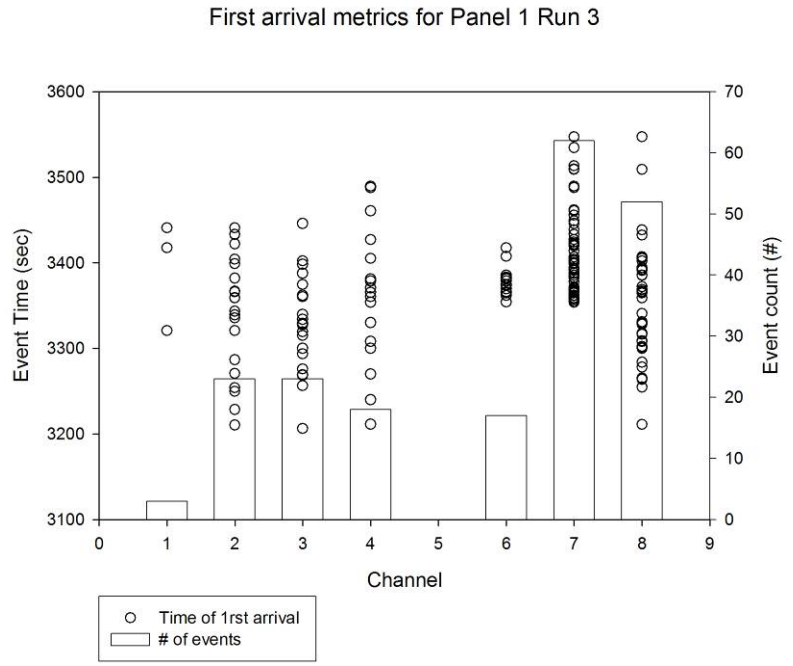

Figure 11 – Identification of sensors that had the most "early" arrivals Panel 1 Run 3

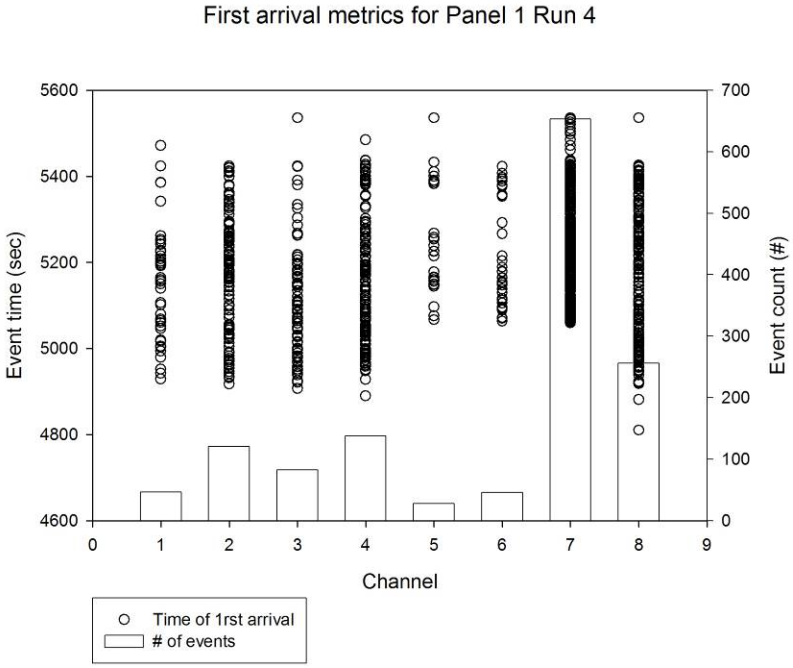

Figure 12 – Identification of sensors that had the most "early" arrivals for Panel 1 Run 4

sensor 8 is in the lower corner of the panel, away from the bracket, this could indicate some composite failure occurring in the lower half of the panel.

This potentially provides the opportunity to identify the AE from the bracket versus the characteristic AE of the composite, i.e. AE that occurs because of internal friction of the composite that isn't primarily the result of damage progression at the loading bracket. So, an attempt was made to eliminate the bolt/bracket noise by identifying those events that would have first arrival on channels 5, 6, and 7. These events were differentiated from the other events and the event locations plotted on a plan view of the panel, as seen in figures 13 and 14. These figures are 2D side views of the test panel as mounted in the test fixture with the same perspective as seen in figures 5, 17, and 30.

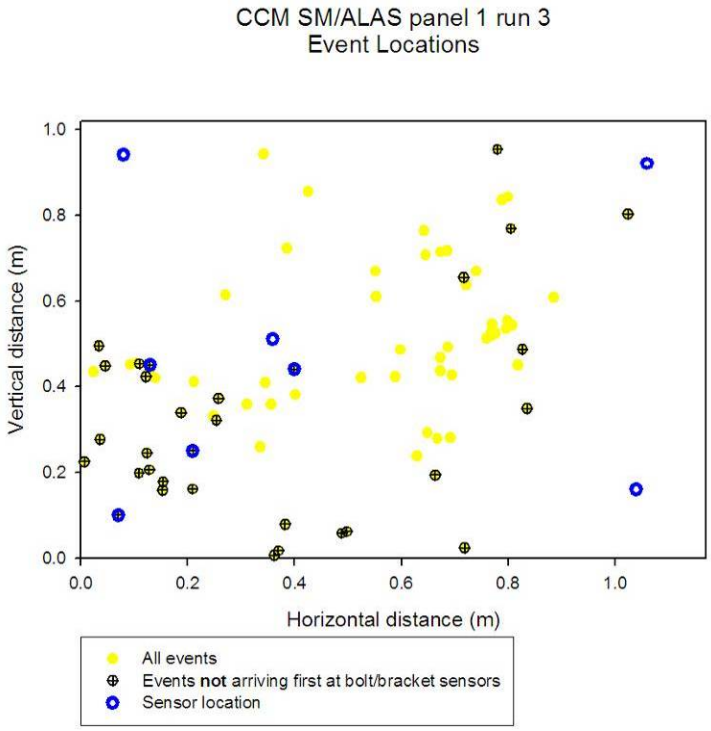

Figure 13 – Identification of bolt /bracket noise for Panel 1 Run 3

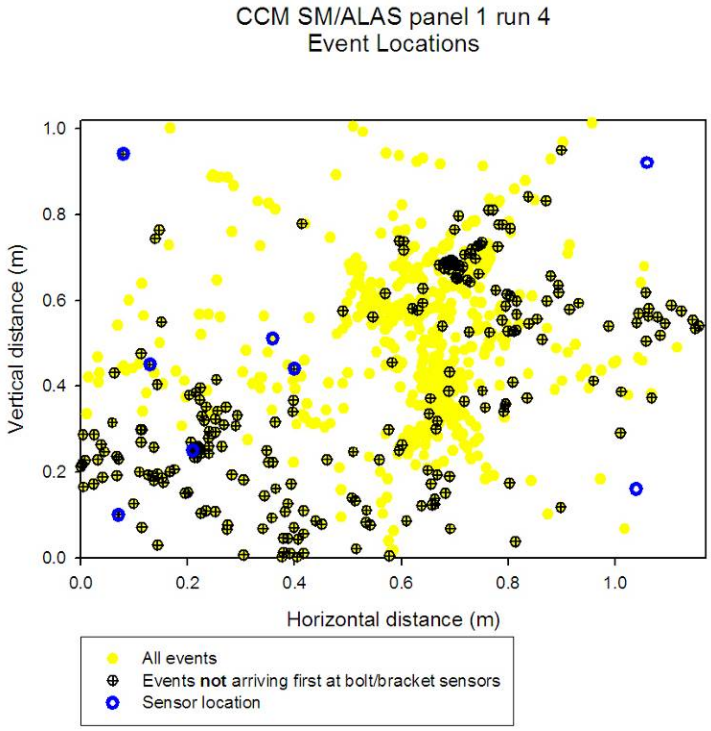

Figure 14 – Identification of bolt /bracket noise for Panel 1 Run 4

It is good to see that the central region of the panel, where the brackets attach, is relatively devoid of events that didn't arrive at the fittings first (black cross-hair). Also, the "bolt/bracket noise" events (yellow) do cluster around the fixture location especially near the end of the fitting where the panel tapers. However, it is noted that there are "bolt/bracket noise" events (yellow) that are located away from the bolt/bracket region and "non-bolt/bracket noise" ones (black) that are located in the bolt/bracket region. This is believed to be due to potential errors in the location calculations that result from difficulty in identifying the first arrival of small signals (i.e. poor signal to noise effects).

It is assumed that most of the loading of panel 1 went to deformation of the bracket and damage around the bracket bolts. If these events are removed by deleting those that have first arrivals at a bolt/bracket sensor, an AE rate characteristic of composite noise under load without bracket mounting damage can be estimated from the remaining plotted events. In figures 15 and 16, one can see that there is a difference in the "characteristic" rates from run 3 compared to run 4 with run 4 having a higher rate. Many of the events of run 4 occur at higher loads (see figure 7) than run 3, so, one could expect that the higher AE rate of run 4 events are more likely to include composite damage events. Conversely, the 0.4 events/second rate of run 3 is possibly related to internal friction. This rate will be compared to the rates from the panel 2 tests later.

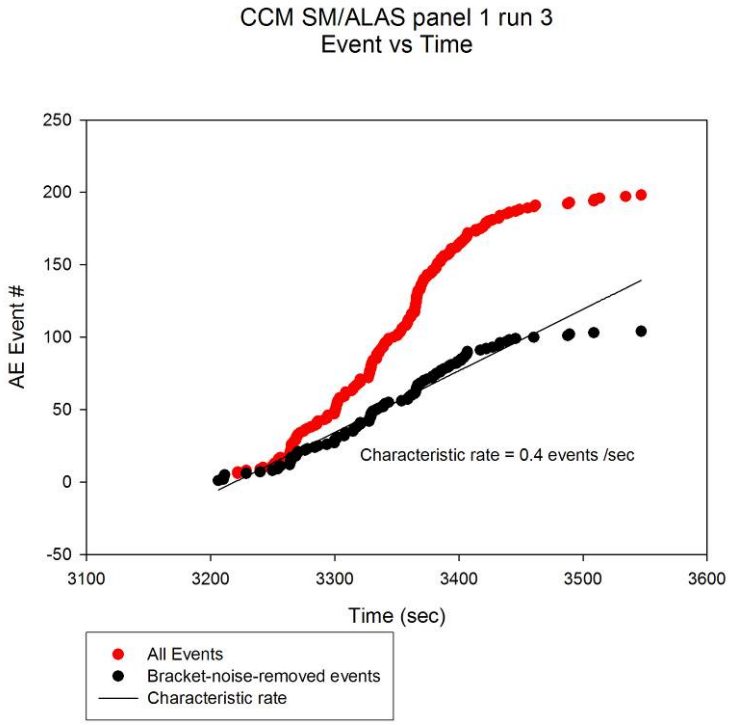

Figure 15 – Investigation of characteristic AE rate: panel 1 run 3

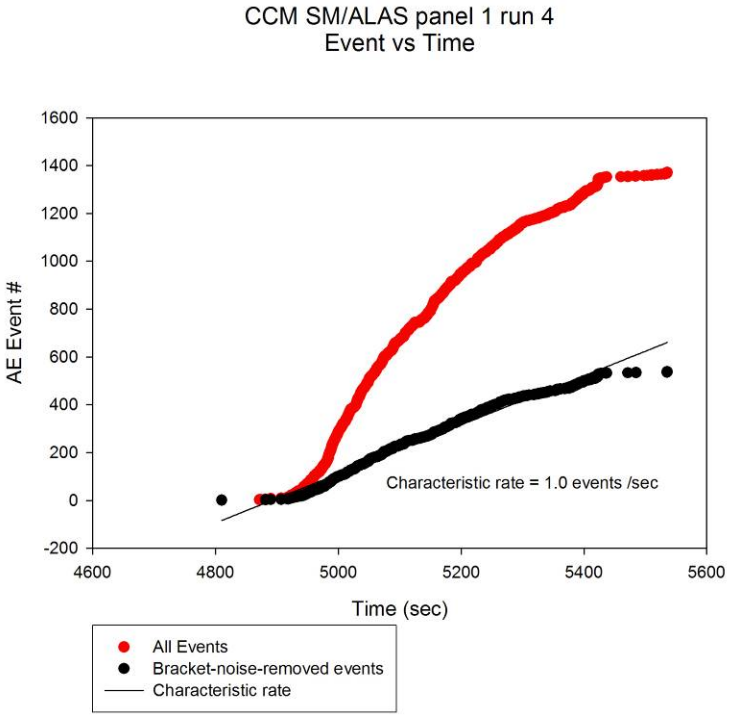

Figure 16 – Investigation of characteristic AE rate: panel 1 run 4

3.2 Panel 2 Analysis

The sensor locations on panel 2, for load testing done on 7/24/08, are approximately the same as was for panel 1 as seen in the following figures 17 and 18. However the boundary sensors have been moved closer to the tapered thickness region of the panel and sensor 6 was relocated between runs 3 and 4 of this test as indicated in figure 18.

Lead breaks were done on the panel near each sensor and the data recorded. A frequency analysis was done on the waveforms of each event and almost all of the energy of the source events (i.e. the waveform collected at sensor nearest the lead-break location) is below 200 kHz. The measured peak frequency of the source is typically in the 70-100 kHz range. However, the energy at the receivers (i.e. waveforms collected at the sensors remote from source) tends to be below 50 kHz. Velocities were calculated using two ranges of band-pass filtering: 10-50 kHz, and 50-100 kHz. To calculate time of arrival, a cross correlation is performed. For this case, the

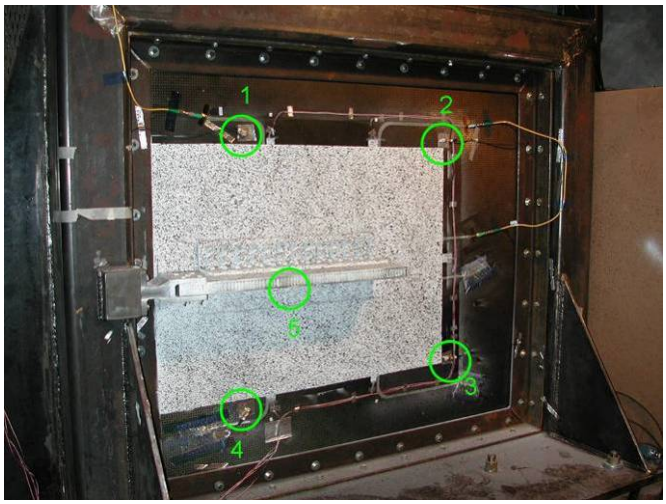

Figure 17 – AE Sensor locations on the back side of panel 2 in test frame

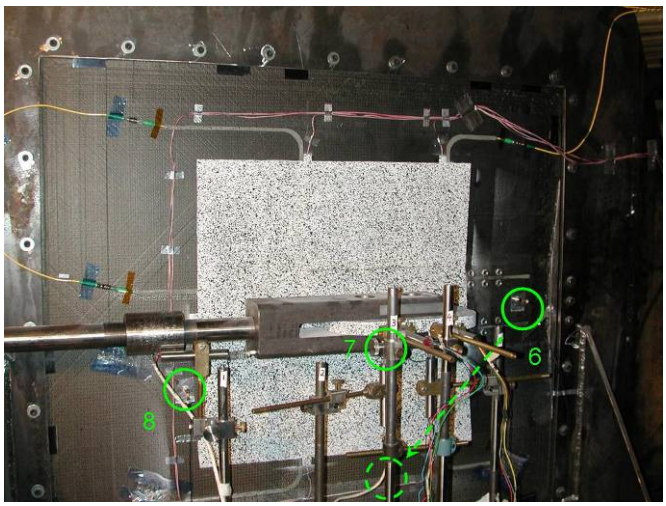

Figure 18 – AE Sensor locations on the front side of panel 2 in test frame

cross correlation is a comparison of a Gaussian pulse of a particular frequency that is shifted in time with the signal. The time of arrival is determined as the time shift that creates the largest correlation value. Knowing the distance between the source and receiver one can then calculate velocity of propagation, which is tabulated in Table 1 below.

A spectrum analysis shows that there can be frequency content at the receivers up to 600 kHz, but it is several orders of magnitude less energetic than the lower frequencies. Inspection of the data from the panel 2 unloading events from run 3 and 5 also shows content in the same two bands: 10-50 kHz and 50-100 kHz. There is a tendency for the signals that travel shorter distances to a sensor, hence arrive earlier, to have more "high" frequency content than the signals that travel farther and arrive at other sensors later. This supports the concept that high frequencies get filtered out quicker with distance, especially in heterogeneous materials, like composites, that have much sound scattering microstructure and significant attenuation. From these results velocities were chosen to be 1300 m/sec for the 10-50 kHz analyses and 1500 m/sec for the 50-100 kHz analyses.

In the following figures 19 and 20 are plots of AE events times plotted against the load profile. The data was not collected in one file as it had been for panel 1. Data acquisition was stopped after run 3 to relocate sensor 6, because there seemed to be substantial AE in the lower portion of the panel. Also, panel 2 did not have bracket failure as did panel 1. Runs 1 and 2 had 2 and 17 events respectively and are not analyzed in depth although the Kaiser effect is noted between runs 1, 2 and 3 as seen in figures 21 and 22. For this panel the "panel" sensors (1, 2, 3, 4, 6, 8) were amplified with a higher gain (54 dB gain) than the "non-panel" sensors (5, 7 @ 42 dB gain). Before relocation of sensor 6 the trigger gain was at 23 dB, but a runaway trigger occurred about halfway through the load hold of run 4 (due to the higher amplitude of the events arriving at sensor 6) so the trigger gain was dropped by 3 dB to 20 dB @ approx. 104 sec during run 4. Changes to trigger gain will affect the number of events that are recorded but not the amplitudes of those events. Due to the Kaiser effect, events in run 4 and 5 are less likely to be damage

Table 1 – Calculation of propagation velocity from sensor to sensor using different filtering parameters

		Band-Pass 50-100kHz, TOA on signal peak amplitude	Band-pass 50-100kHz, x-corr. on 75kHz, TOA on peak	Band-pass 10-50kHz, TOA on peak	Band-pass 10-50kHz, x-corr. on 30kHz, TOA on peak
source	receiver	velocity (m/s)	velocity (m/s)	velocity (m/s)	velocity (m/s)
1	2	1273	1476	1068	1289
2	1	1331	1331	1268	1268
2	3	1370	1503	1347	1287
3	2	1358	1479	1060	1258
3	4	1487	1529	1437	1393
3	8	343	344	215	219
1	6	1107	1116	1398	810
1	7	1619	1492	909	909
2	8	1436	1453	1293	1173
3	7	971	942	840	888

events since run 3 had “preconditioned” this panel with a peak load of 24 kips, whereas 4 and 5 only went to 8 and 14 kips respectively.

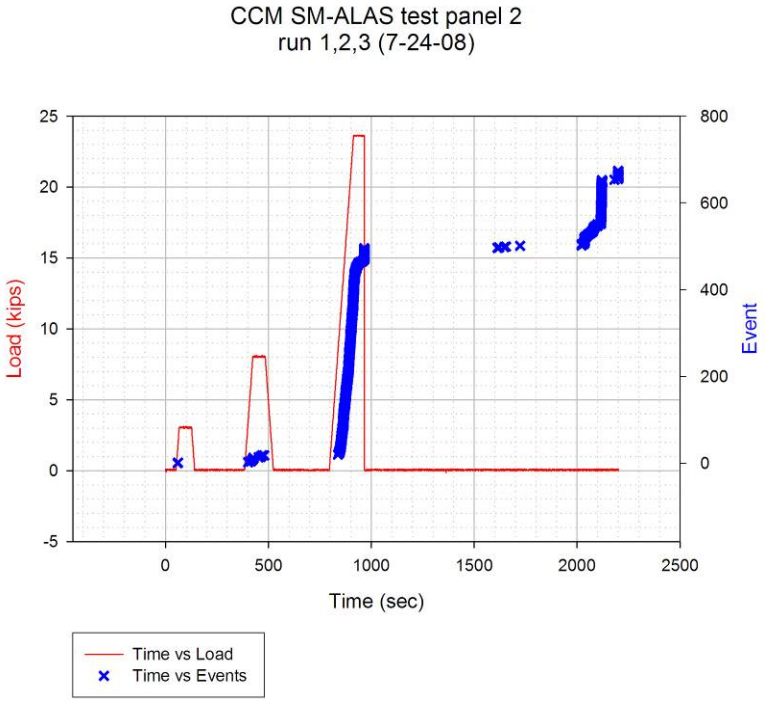

Figure 19 – Acoustic emission rate vs. load profile for panel 2 runs 1-3

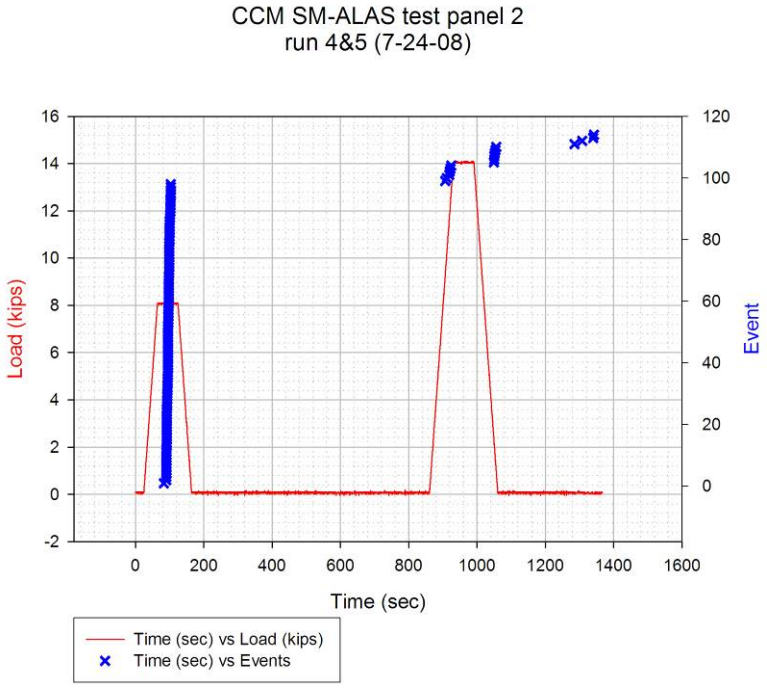

Figure 20 – Acoustic emission rate vs. load profile for panel 2 runs 4 and 5

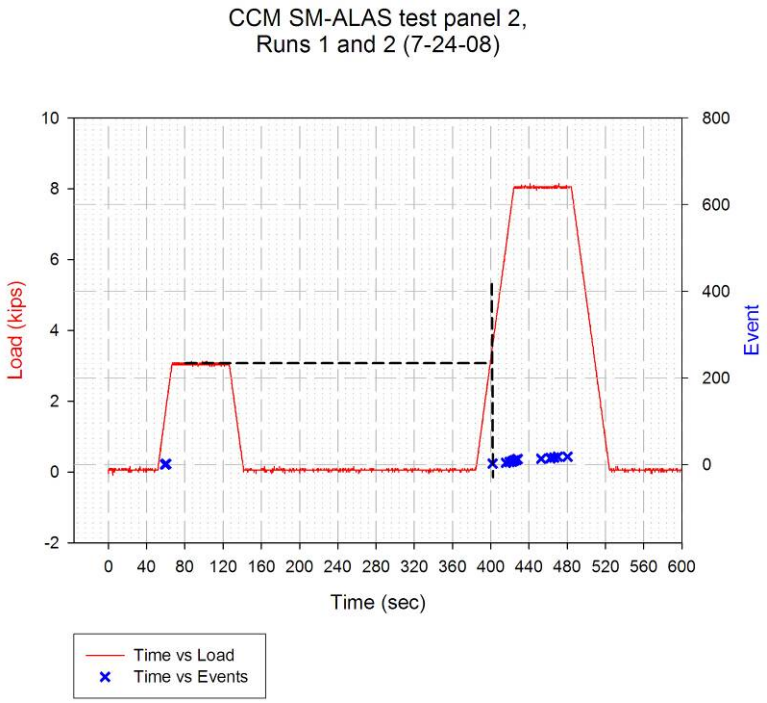

Figure 21 – Kaiser Effect between load cycles (runs) 1 and 2 of panel 2 test

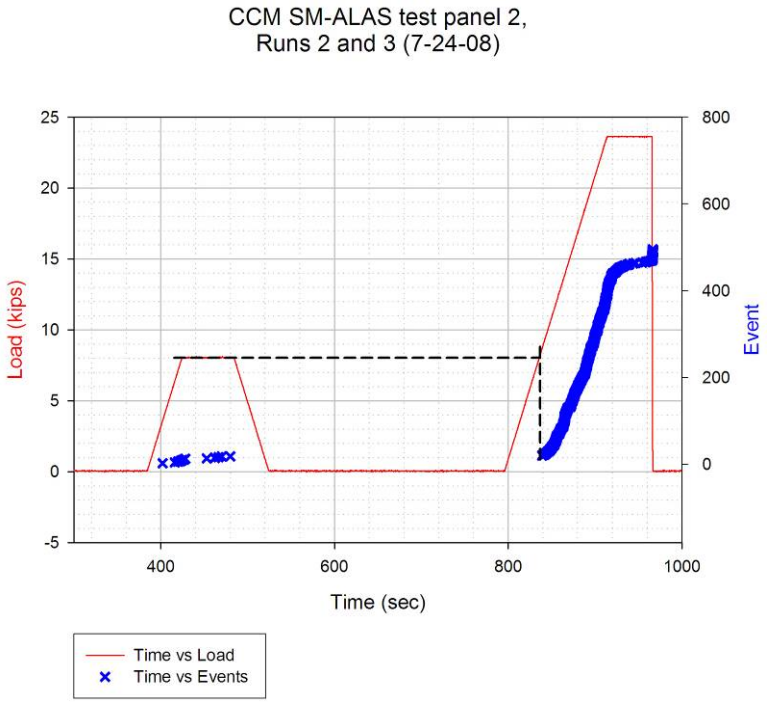

Figure 22 – Kaiser Effect between load cycles (runs) 2 and 3 of panel 2 tests.

As noted previously the five runs (1-5) produced 2, 17, 477, 98, and 12 AE events respectively. The following figures 23, 24 and 25 show the event time of the first sensor arrival and the histogram of the first arrival event count, both plotted per channel (sensor). As noted above, run 3 was the run likely to develop the most damage and this is supported by this run having at least 5 times more events than the other runs. It is interesting to note that for runs 2 and 4 the region near the corners of the potted core, where sensors 2 and 3 are, dominates the data. However, it may be ill-advised to draw too many conclusions because of the low event count for both of those runs.

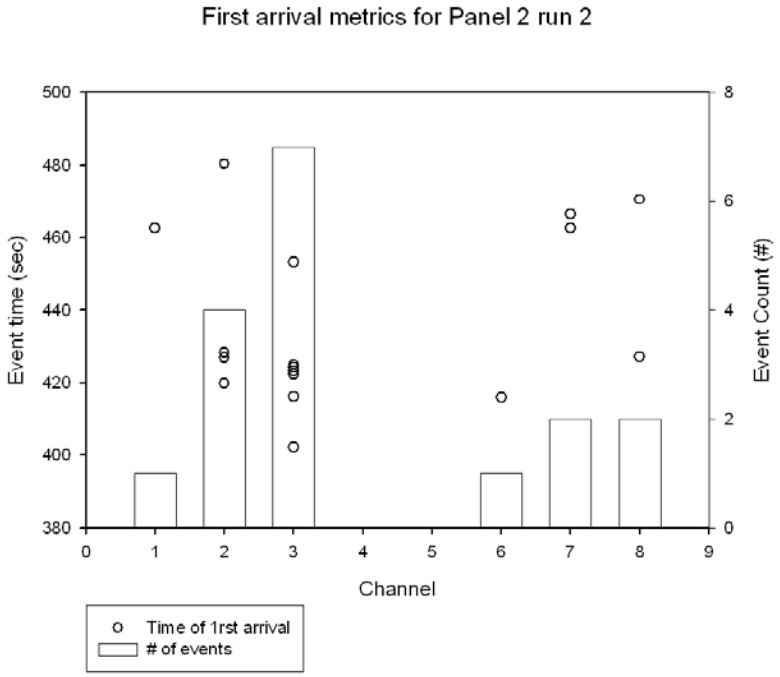

Figure 23 - Identification of sensors that had the most "early" arrivals Panel 2 Run 2

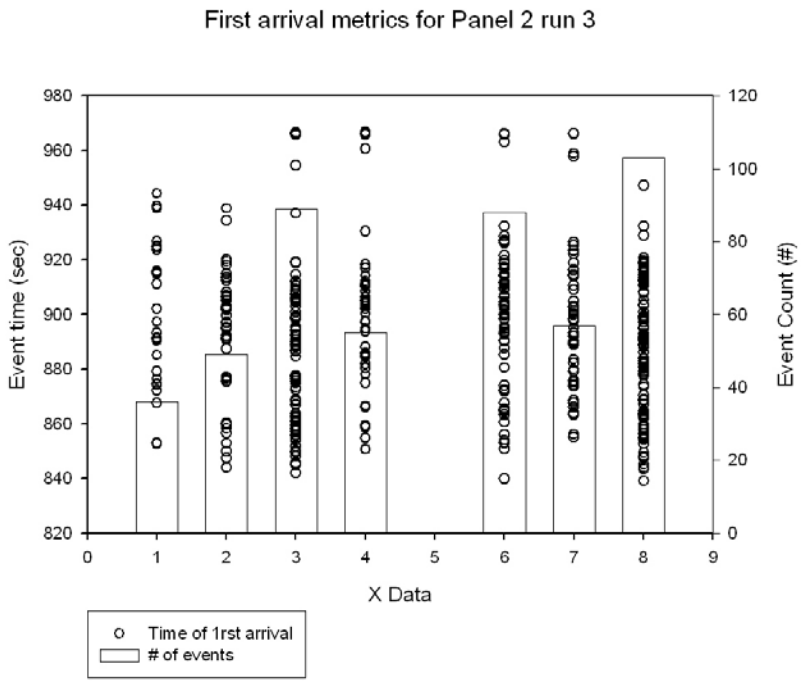

Figure 24 - Identification of sensors that had the most "early" arrivals Panel 2 Run 3

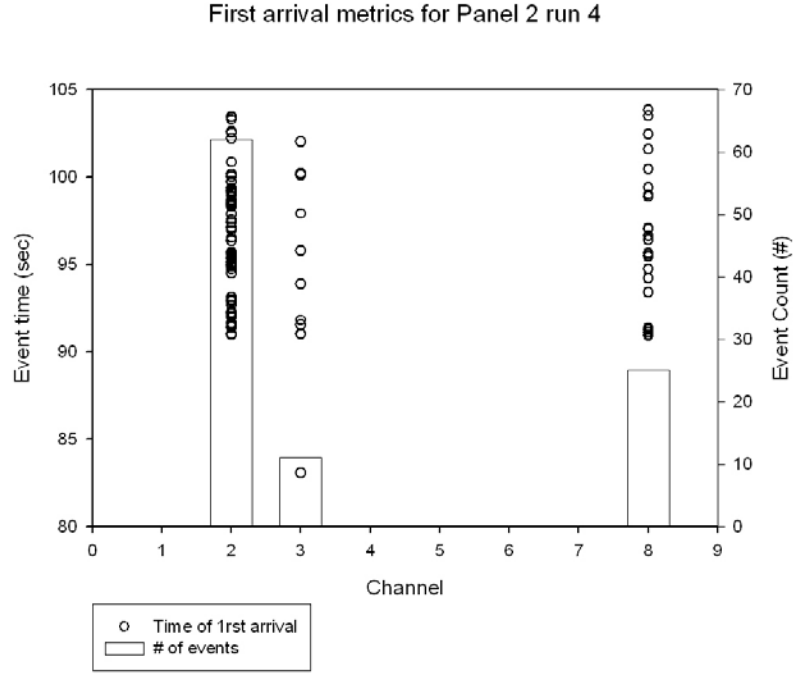

Figure 25 - Identification of sensors that had the most "early" arrivals Panel 2 Run 4

Unloading Events

In the following figures 26 and 27, plots of AE vs. time overlaid on the load profiles of runs 3 and 5 show the unloading events (events that occurred during unloading). These events have the

potential to locate where damage in a composite has occurred during previous loadings because of the increased internal friction in the region of the damage.

The source locations of these unloading events were calculated and are plotted in figures 28 and 29. The figures are 2D side views of the test panel in the test fixture with the same perspective as seen in figures 5, 17, and 30.

Note that the locations definitely cluster in the lower half of the panel. Figure 30 shows a postmortem C-scan of panel 2 and as noted in the cut plan for destructively examining the panel " white areas in the scan are where the threshold was not exceeded, meaning essentially no sound is coupled through the panel." [3] That means that either delamination in the composite or debonding of skin in the regions of honeycomb core had occurred. Most of the lower half of the panel has that damage. It is very likely that internal friction of the damage contributed to the unloading events. This indicates that the damage was present prior to the unloading of run 3. The large number of events during loading in run 3 could indicate the occurrence of the damage, although as seen in later plots locations of the events do not definitively highlight the damage regions. However, that could be due to the fact that the damage covers almost 75% of the panel.

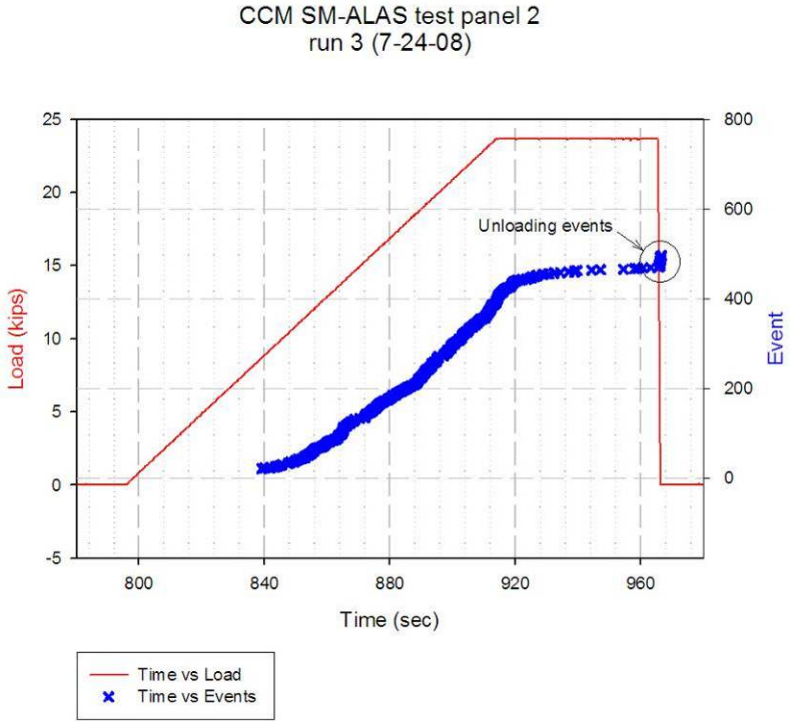

Figure 26 – Events that occurred during unloading for panel 2 run 3.

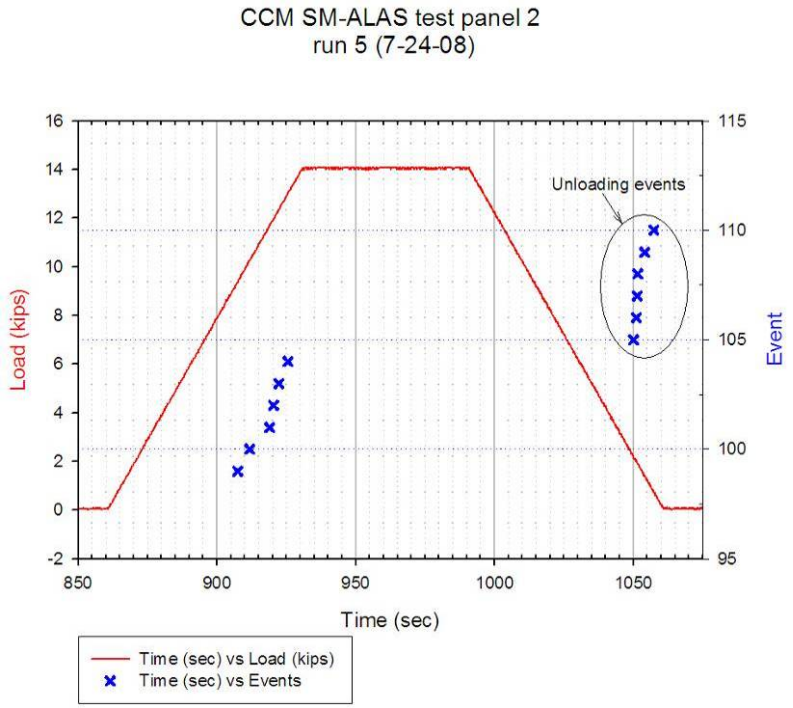

Figure 27 – Events that occurred during unloading for panel 2 run 5.

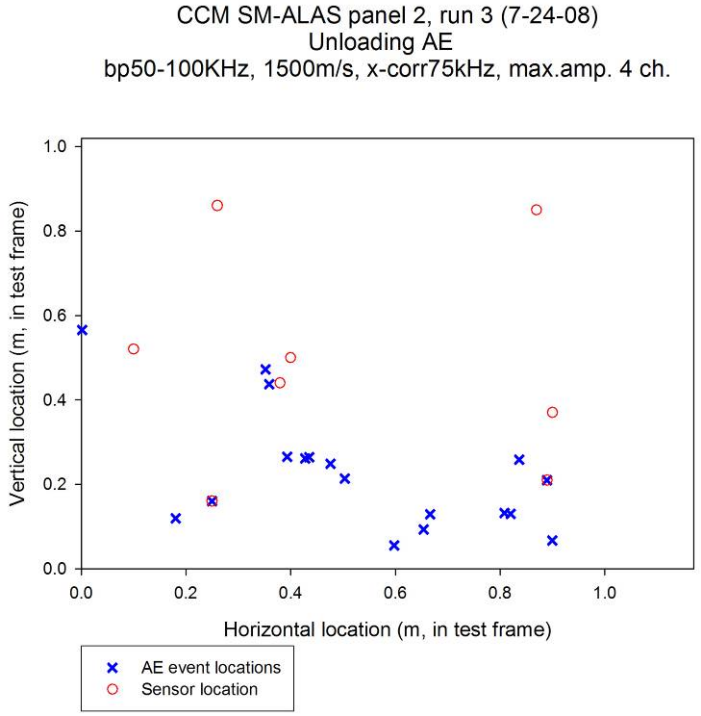

Figure 28 – Locations of unloading events for panel 2 run 3

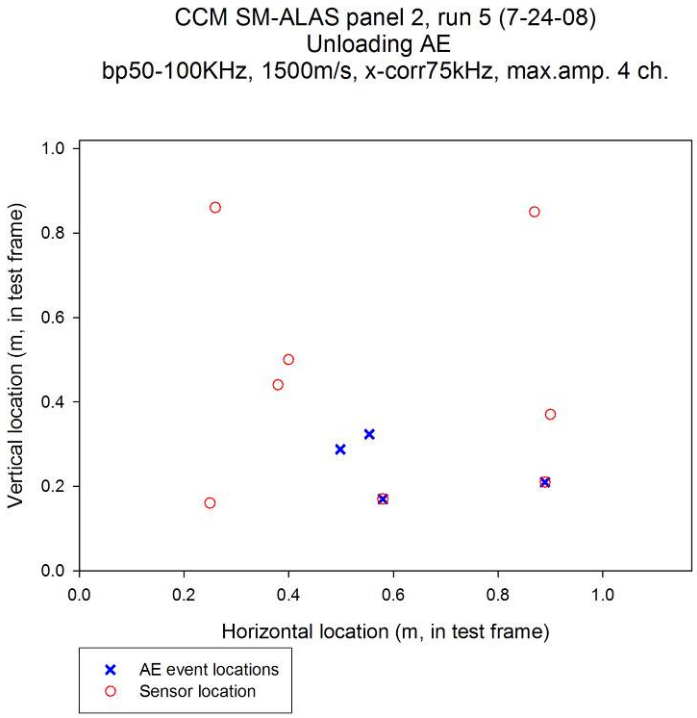

Figure 29 – Locations of unloading events for panel 2 run 5

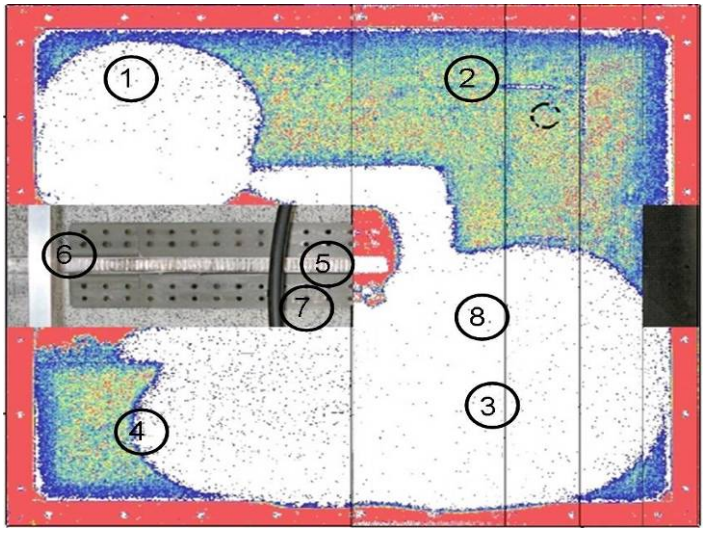

Figure 30 – Post-mortem c-scan of panel 2 showing large area of delamination (white region) of skin from core

Event Energy

Figures 31-35 are AE energy plots for panel 2. The source is the original unfiltered data. However, extraneous events that did not occur during a load cycle have not been plotted. The signal energy, *SE*, is calculated from the signal as

$$SE = \frac{1}{R}\sum_{i=1}^{n} V_i^2 \Delta t$$

where V is the signal voltage, R is the input impedance (for simplicity, R is often taken as the input impedance of the just the input amplifier because the transducer's impedance can vary significantly and may not be known), i is the time reference point, n is the number of time points in the signal, which in this test was 8192 points corresponding to 1638 μs, Δt is the sampling time per point.

One can see in figure 33 of the event energy for run 3 the peak energies are at least an order of magnitude larger than any of the other runs for panel 2. Also one sees energy increases with time during loading, until the load hold starts at approximately 920 seconds. This increase can be indicative of damage development because of increasing energy release during loading.

It was previously noted that events during run 4 were unlikely to be damage events due to the Kaiser effect. The energy plot for those events as seen in figure 34 also supports this. During the run 4, as noted previously, runaway triggering was occurring and the trigger gain was reduced toward the end of the run to alleviate that. The very low values of energy, at least two orders of magnitude less than runs 5 and 3, support the concept of non-damaging sources. The results also show distinct segregation by channel into energy bands which would also imply a single repeating non-damaging source of constant amplitude, because the distance traveled from a single source to sensor and hence the attenuation would be the same for every event arriving at a particular sensor.

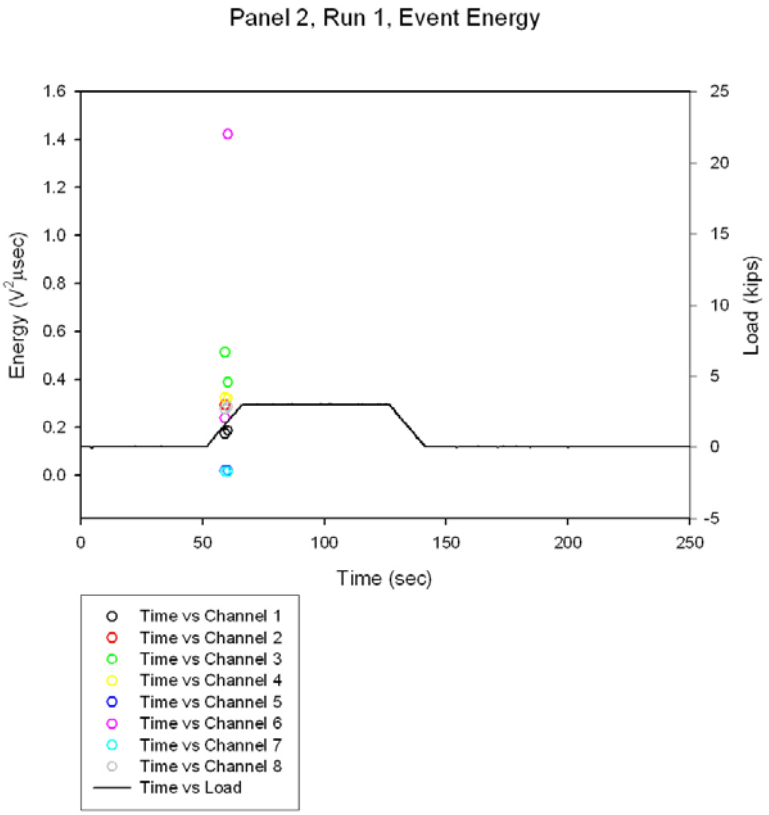

Figure 31 – Calculated energy of each AE event plotted by channel (sensor) and time for panel 2 run 1

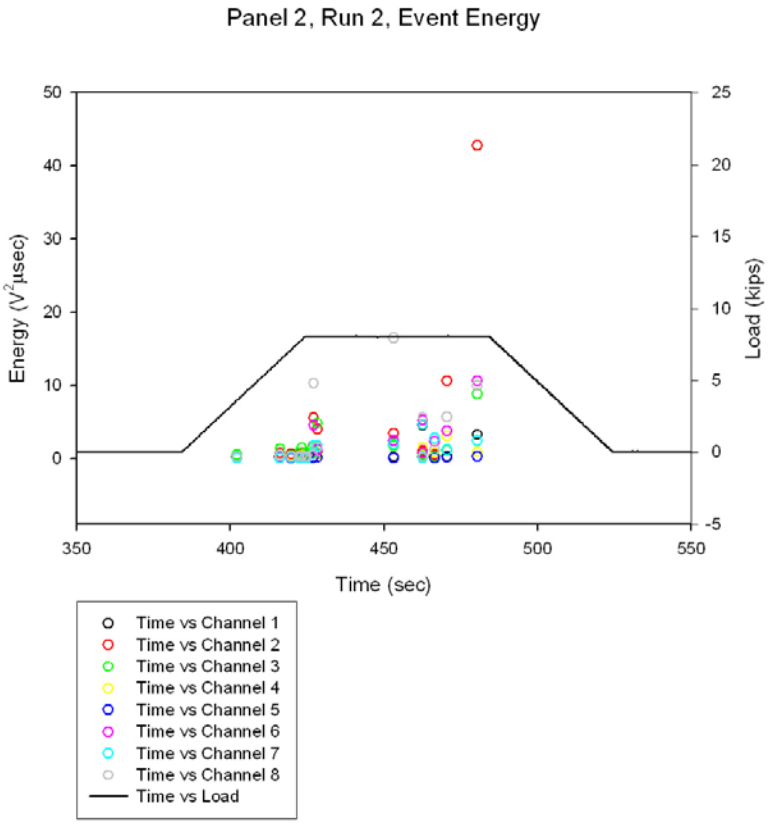

Figure 32 – Calculated energy of each AE event plotted by channel (sensor) and time for panel 2 run 2

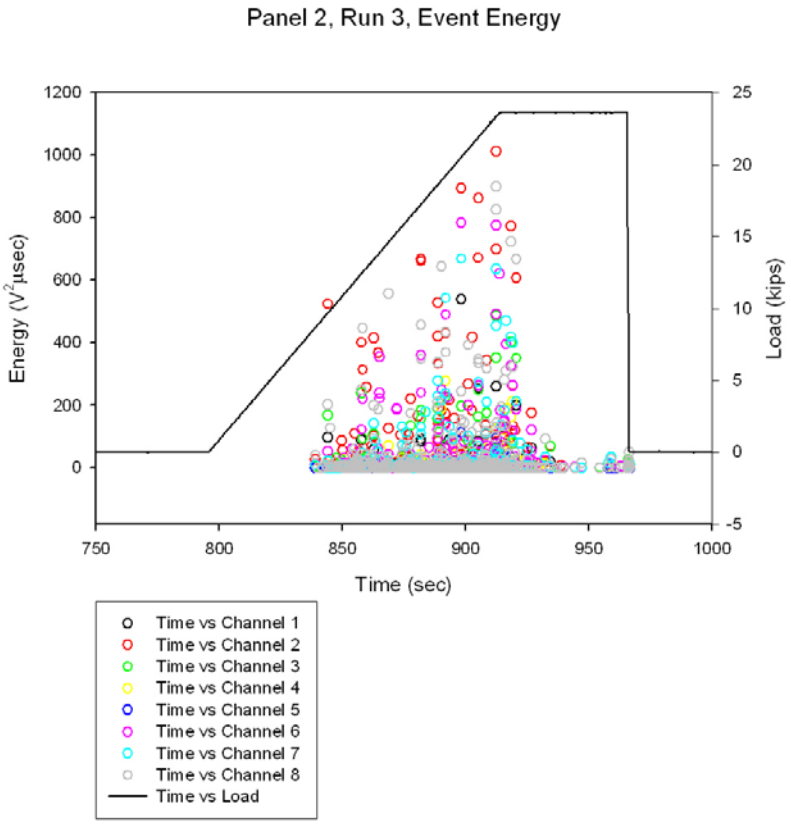

Figure 33 – Calculated energy of each AE event plotted by channel (sensor) and time for panel 2 run 3

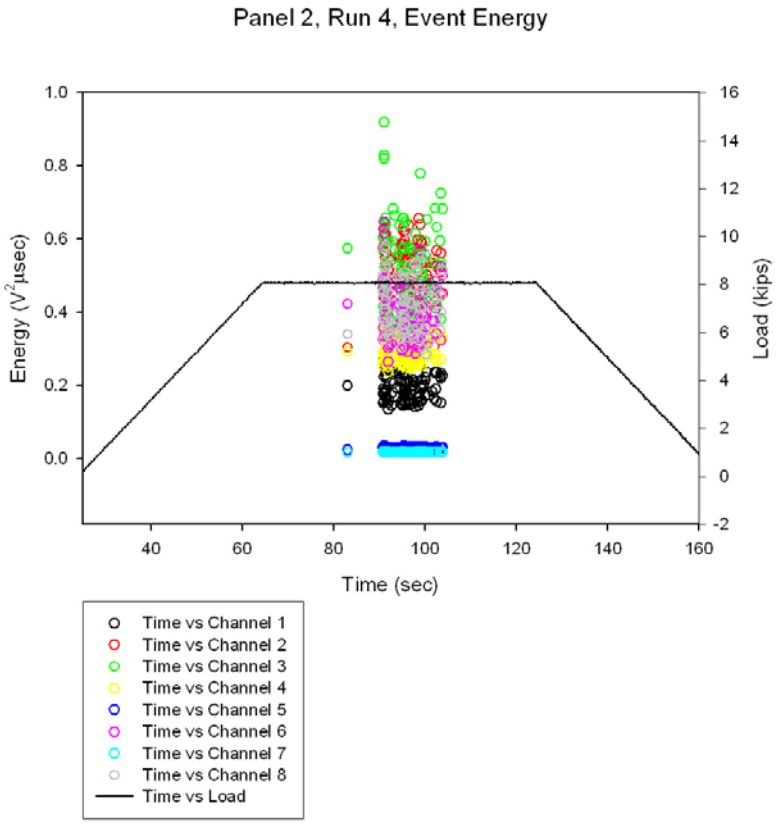

Figure 34 – Calculated energy of each AE event plotted by channel (sensor) and time for panel 2 run 4

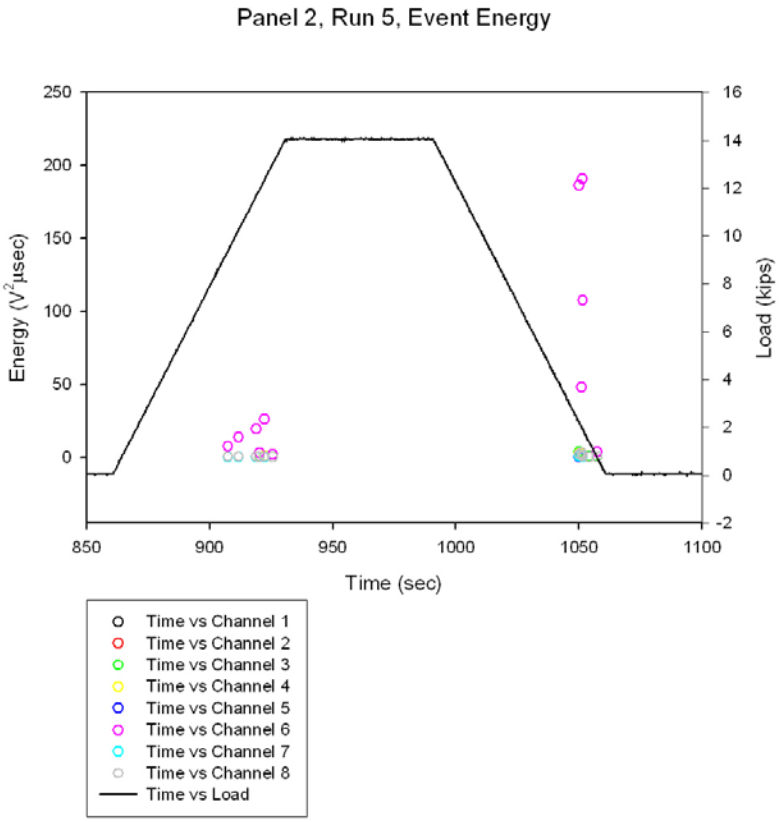

Figure 35 – Calculated energy of each AE event plotted by channel (sensor) and time for panel 2 run 5

Event locations

As noted in the section for Panel 1 results, two analyses were used to calculate locations, one using a velocity of 1300 m/s and bandpass filtering between 10 and 50 kHz zone, the other 1500 m/s and 50-100 kHz. Although the calculated locations between the two analyses are not identical, the patterning is very similar, so only the 1500 m/s analyses are shown in the following discussions

Because of the small number of low energy events for runs 1 and 2 the location of all the events for runs 1, 2, and 3 are plotted together in Figure 36. The figure is a 2D side view of the test panel in the test fixture with the same perspective as seen in figures 5, 17, and 30.

Run 3 had the largest number of events of all the runs and they were spread over most of the load profile. It was felt that indicating the time and location of the event may provide some information concerning the damage development. Figure 37 shows the location plot that has the events colored to indicate what portion of the load profile it occurred in. The profile was divided approximately into quarters, as seen in Figure 38, with the first quarter containing essentially no events and the last quarter containing the load hold and unloading events. The scattering is broad but it does look like the events tended to occur near the right half of the panel schematic earlier in the test and moved toward the left and down with time.

It was suggested previously that the events from run 4 are likely to be from a single non-damaging source. However, the location calculations as seen in figure 39 are scattered with approximately 40% of all the event locations either not calculable or located well outside the frame. This is most likely due to the low energy levels making it difficult to calculate the signal time arrival at each sensor.

The events of run 5 cluster in the bottom half of the panel toward the center as seen in figure 40. This correlates reasonably well with the location of the later events in runs 1-3.

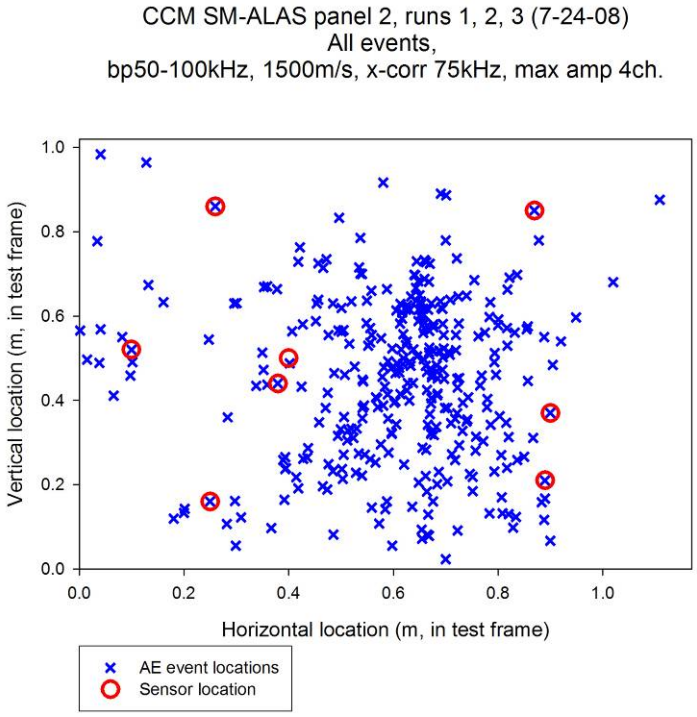

Figure 36 – Combined plot of event locations for runs 1-3

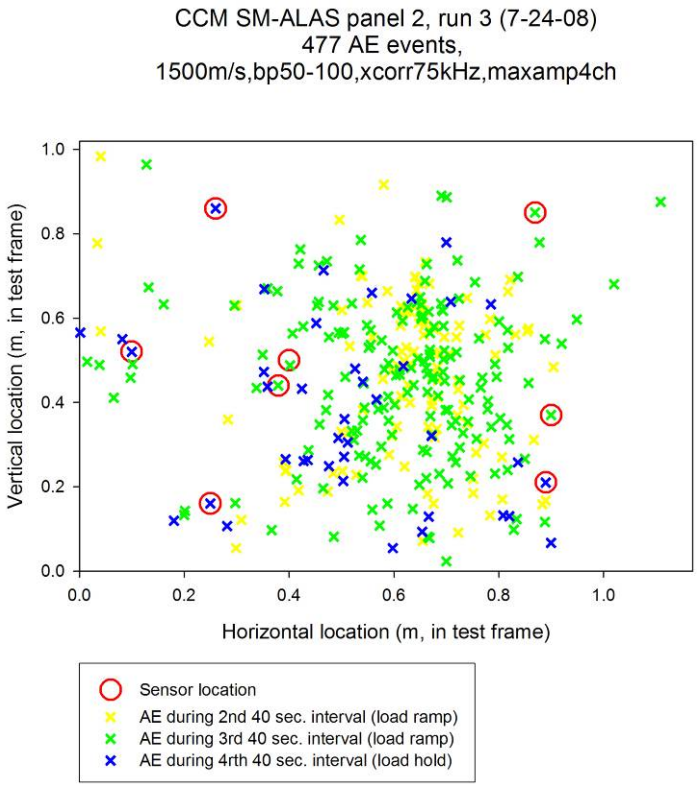

Figure 37 – Time and location plot of events for run 3

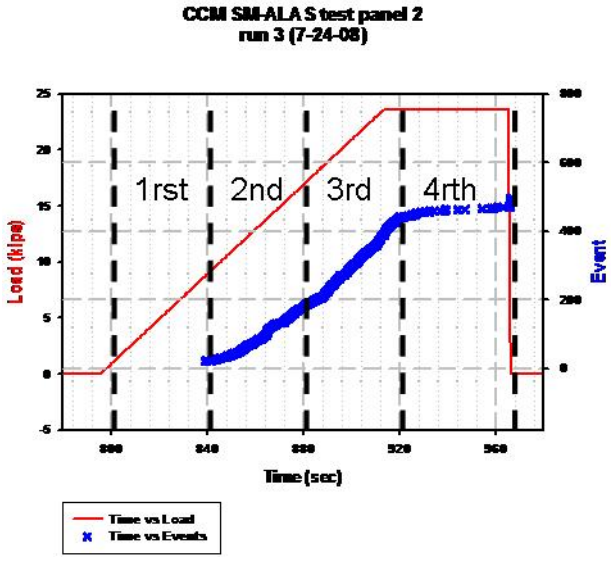

Figure 38 – Division of run 3 into 4 time bins.

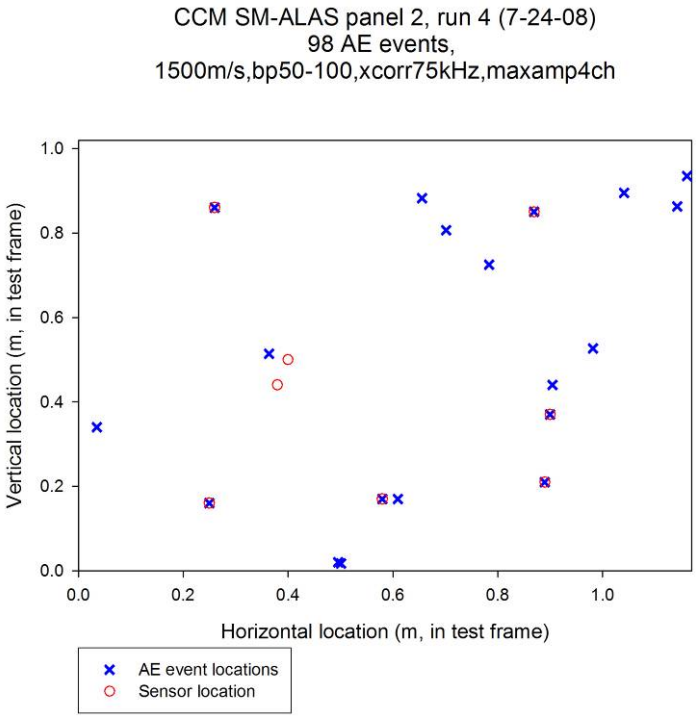

Figure 39 – Event location plot for run 4

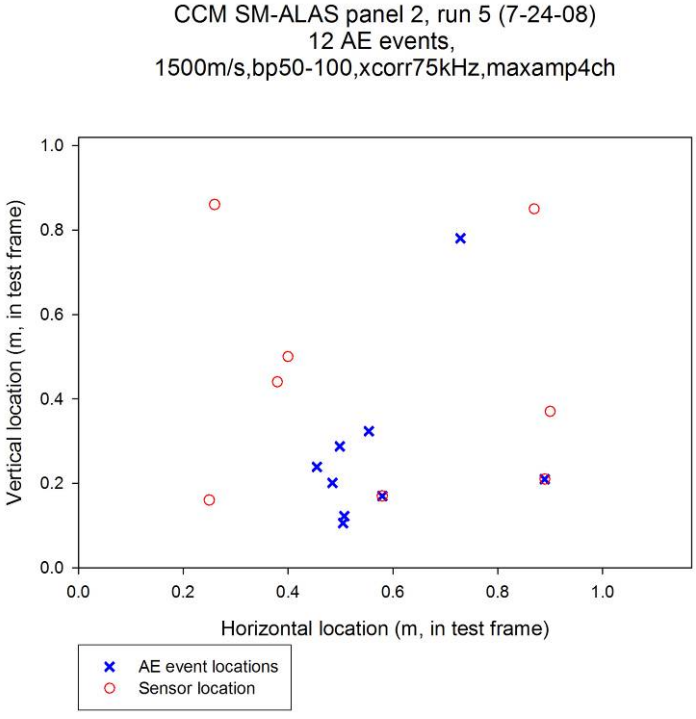

Figure 40 –Event location plot for run 5

Event Rates

In figures 41 and 42 are plotted the event rates for panel 2 runs 3 and 4. Comparing these to the rate from panel 1 (0.4 events/second), only the AE occurring during the load hold of run 3 is comparable. The AE rates during loading for both runs 3 and 4 are an order of magnitude higher. It might be suggested that run 3 was damage and the slightly higher rate of run 4 was also damage, but, as noted previously, the energy and location results suggest otherwise for run 4.

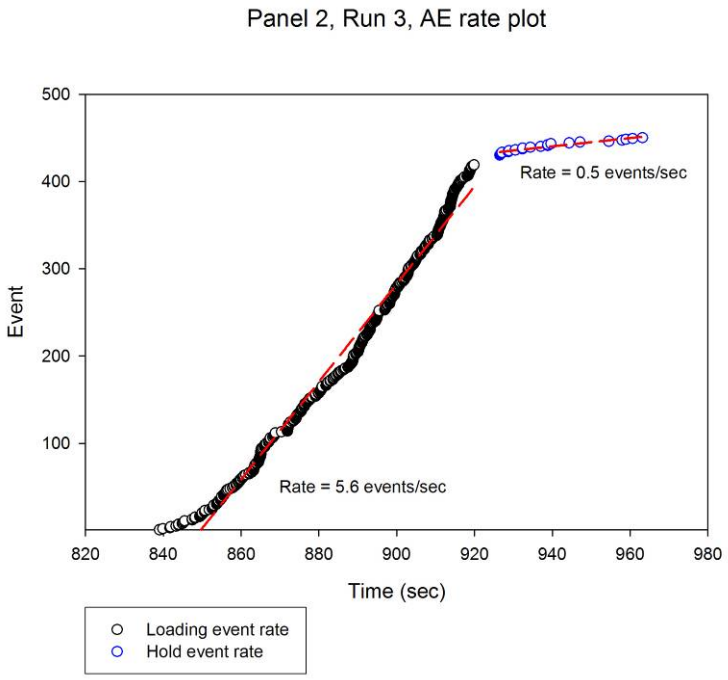

Figure 41 –Event rates for run3

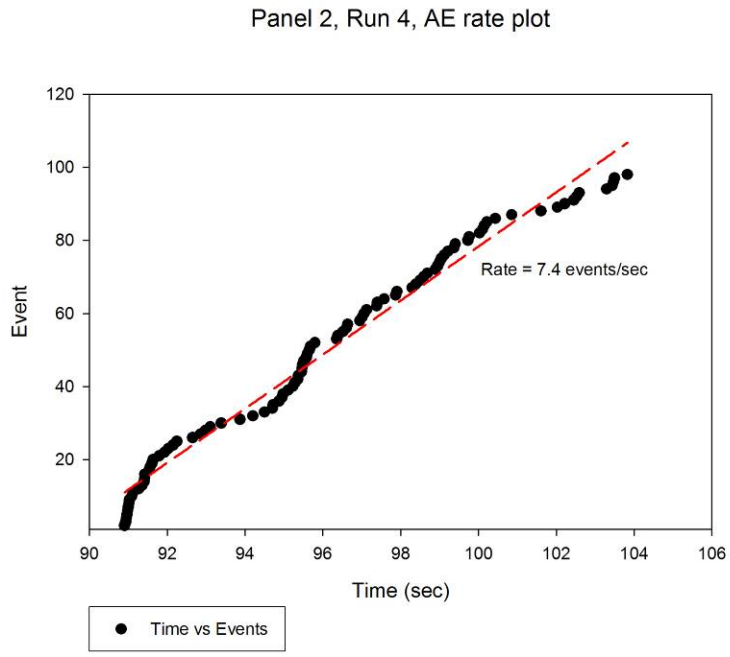

Figure 42 –Event rate for run 4

4.0 Lessons Learned, Summary, and Conclusions

In AE research, the Kaiser effect typically considers that if no damage has occurred since a previous load cycle, then acoustic emission will not occur during a subsequent load cycle until the peak load of the previous cycle has been reached. It is primarily valid for metallic materials and typically is only approximate for composite materials due to their more complex microstructure and localized plasticity. Hence re-emitting due to internal friction can occur during subsequent loading at lower than peak loads. It would only be applicable to this composite's heterogeneous structure to the extent that the results show that the structure is "conditioned" by loading. This conditioning does affect the generation of AE in later load cycles. However, the first few cycles of Panel 1 conformed closely to the Kaiser effect. This suggested a metallic failure was occurring, which indeed was the case.

Ramifications of the Kaiser effect or "load conditioning" are many. All clevises, grips, fixtures and loading components of a test frame could possibly create AE unless they were pre-loaded with a dummy component to at least maximum test load before testing the real component. However, because the new component then has to be bolted into the test frame, eliminating settling-in AE is difficult. Use of procedures to eliminate pre-stress in the component during mounting is helpful. It should also be kept in mind that test procedures can affect AE. Monitoring a single load cycle from virgin condition to full test load could enhance the interpretation of trends in the AE. However, multiple cycles with increasing peak loads may be needed to indicate continuing damage development or localization in fatigue. In other words, how a test proceeds, from setup to finale, should be taken into account when interpreting the data.

Panel 1: It was shown that that the majority of the events occurred near the bracket mounted sensor 7 which correlates well with the failure of metallic bracket. A significant burst of that AE occurred in Run 3 at loads between 15 and 30 kips, but the majority was above 30 kips in Run 4. The percentage of first arrival hits at sensor 8 comes in second after sensor 7 for both runs. This could indicate some composite failures occurring in the lower half of the panel. Event locations support the conjecture that most of the events were bracket failure. Eliminating those bracket events and examining the remaining events allowed estimation of the characteristic rates of AE from composite deformation.

Panel 2: Looking at the energy plots suggests that the panel was prematurely weak such that much of the damage was occurring at loads well below 15 kips during run 3. The events of runs 1 and 2 are much lower energy and quantity than those of run 3. The highest energies of run 3 occurred at sensors 2, 8, 6, and 7 in the "upper half" of the panel (as viewed in the testing configuration). Sensors 2, 8, 6, and 7 tend to outline a region which is only partially delaminated as noted in the post mortem C-scan of panel 2. This, in conjunction with the high energy AE, suggests that this region of delamination grew during the test. In contrast, sensors 1, 3 and 4 that are in or at the edge of delamination had lower energies, suggesting that these regions of delamination was a preexisting condition. Run 5 also had high energy events, but not the quantity, suggesting that most of the damage had already occurred in run 3.

Panel 2 seemed weak at well below 15 kips while panel 1 AE indicates the bracket failure didn't start until 15 kips. It is unclear what was happening to panel 2 between 15 and 30 kips. The debonded region surrounds the bracket region so it is difficult to sort out bracket noise from debonding noise by location.

In summary, the results of this analysis in comparison with other information, such as the post mortem C-scan outlining the debonded region, is self-consistent.

References

[1] Composite Crew Module (CCM), Simplified SM/ALAS TEST PLAN, June 24, 2008, Prepared by: Chip McCann, NASA/JSC".
[2] Pollock, A. Acoustic Emission Inspection. In ASM Handbook, V17 Nondestructive Evaluation and Quality Control, V
[3] Personal communication with Sotiris Kellas

REPORT DOCUMENTATION PAGE

Form Approved
OMB No. 0704-0188

1. REPORT DATE *(DD-MM-YYYY)*	2. REPORT TYPE	3. DATES COVERED *(From - To)*
01- 10 - 2010	Technical Memorandum	

4. TITLE AND SUBTITLE

Evaluation of Acoustic Emission NDE of Composite Crew Module Service Module / Alternate Launch Abort System (CCM SM/ALAS) Test Article Failure Tests

5a. CONTRACT NUMBER

5b. GRANT NUMBER

5c. PROGRAM ELEMENT NUMBER

6. AUTHOR(S)

Horne, Michael R.; Madaras, Eric I.

5d. PROJECT NUMBER

5e. TASK NUMBER

5f. WORK UNIT NUMBER

724297.40.44.07

7. PERFORMING ORGANIZATION NAME(S) AND ADDRESS(ES)

NASA Langley Research Center
Hampton, VA 23681-2199

8. PERFORMING ORGANIZATION REPORT NUMBER

L-19930

9. SPONSORING/MONITORING AGENCY NAME(S) AND ADDRESS(ES)

National Aeronautics and Space Administration
Washington, DC 20546-0001

10. SPONSOR/MONITOR'S ACRONYM(S)

NASA

11. SPONSOR/MONITOR'S REPORT NUMBER(S)

NASA/TM-2010-216859

12. DISTRIBUTION/AVAILABILITY STATEMENT

Unclassified - Unlimited
Subject Category 16
Availability: NASA CASI (443) 757-5802

13. SUPPLEMENTARY NOTES

14. ABSTRACT

Failure tests of CCM SM/ALAS (Composite Crew Module Service Module / Alternate Launch Abort System) composite panels were conducted during July 10, 2008 and July 24, 2008 at Langley Research Center. This is a report of the analysis of the Acoustic Emission (AE) data collected during those tests.

15. SUBJECT TERMS

Launch Abort System; Acoustic emission

16. SECURITY CLASSIFICATION OF:			17. LIMITATION OF ABSTRACT	18. NUMBER OF PAGES	19a. NAME OF RESPONSIBLE PERSON
a. REPORT	b. ABSTRACT	c. THIS PAGE			STI Help Desk (email: help@sti.nasa.gov)
					19b. TELEPHONE NUMBER *(Include area code)*
U	U	U	UU	41	(443) 757-5802